Colloid Polym Sci 276:1098–1109 (1998)

ORIGINAL CONTRIBUTION

H. Binder
B. Kohlstrunk
U. Brenn
W. Schwieger
G. Klose

Infrared dichroism measurements on the alkyl chain packing of an ionic detergent intercalated between silicate layers

Received: 14 January 1998
Accepted: 27 July 1998

Dr. H. Binder (✉) · B. Kohlstrunk
G. Klose
Universität Leipzig
Fakultät für Physik
Institut für Experimentélle Physik I
Linnéstr. 5
D-04103 Leipzig
Germany
e-mail: binder@rz.uni-leipzig.de

U. Brenn · W. Schwieger
Martin-Luther-Universität
Halle-Wittenberg
Institut für Technische Chemie
und Makromolekulare Chemie
Schloßberg 2
D-06108 Halle
Germany

Abstract Microcrystals of the metal silicate hydrate ilerite orient macroscopically on the surface of a ATR-crystals and thus, are accessible for infrared linear dichroism measurements. We present first results which indicate that the alkyl chain packing and the orientation of the polar group of dodecyltrimethylammoniumbromide (DTAB) intercalated between silicate layers can be determined in terms of infrared order parameters. The properties of DTAB can be modulated by the relative humidity of the surrounding atmosphere and by temperature. Upon heating DTAB undergoes a phase transition from a paraffin-like solid to a fluid phase. The former is characterized by the orthorhombic perpendicular packing of the frozen alkyl chains with tilted long axes. The interactions between the ionic groups of the surfactant and that of the host matrix stabilize the lamellar arrangement of DTAB in the crystalline and in the fluid phases.

Key words Metal silicate hydrate layers – infrared linear dichroism – order parameter – orthorhombic subcell – tilt angle – trimethylammonium group

Introduction

Inorganic layered materials as e.g. mineral clays or metal silicate hydrates with detergents intercalated between them combine properties of "soft" and "hard" matter. The detergent forms a viscous, hydrophobic interior the physico-chemical properties of which can be modulated by external parameters as relative humidity and temperature. The inorganic layers represent a rigid "boundary" which confines the detergents. Beside their potential applications as a host matrix for hydrophobic solutes these systems have been the focus of fundamental research on the basic principles of microconstrained amphiphilic aggregation and phase behavior. The partial arrangement of the detergent molecules can be viewed as a compromise between the constraints which exert the inorganic crystalline network on detergent head group packing via, e.g., coulombic interactions or H-bonding on the one hand and the structural properties of the hydrophobic core which are characterized by the conformation and arrangement of the alkyl chains, on the other hand [1]. For example, alkylammonium cations are known to adopt a paraffin-type interlayer arrangement with a high degree of regularity where the geometrical constraints can however only be fulfilled for certain combinations of tilt angles and chain packing densities [2–5]. Beside the all-trans conformation of the alkyl chains also kink- and gauche-blocks [6], end-gauche defects [7] or U-shaped chain conformations [8] are discussed on the basis of basal spacings obtained by means of X-ray scattering, the method which is frequently applied for structural studies on inorganic layers.

Also vibrational spectroscopy has been used since many years to investigate the structural details of the inorganic network of silicate layers [9] and to determine

the nature of bonding of several intercalates [10, 11]. Although infrared (IR) and Raman spectroscopy represent powerful and well-developed techniques to characterize liquid and crystalline hydrocarbons [12–16] as well as amphiphilic aggregates [17–20] on a microscopic level they were only scarcely used to investigate alkyl chain properties of intercalates [21].

The present paper reports the first IR dichroism measurements on a synthetic sodium octosilicate hydrate (SiO_2/Na_2O mol ratio ≈ 8) which has been called ilerite [22, 23] with intercalated alkylammonium ions. This method could be applied because we succeeded in preparing powdered samples of non-aggregated plate-like crystallites which orient spontaneously on flat surfaces. The results will demonstrate the capability of infrared spectroscopy to highlight structural details of the alkyl chain arrangement on a molecular level and simultaneously to detect phase transitions. In particular, we show that the orientation and packing mode of the alkyl chains can be extracted from the spectral data. Unfortunately, the dichroism of the intense methylene stretching bands is only inadequately understood on a quantitative level at present and thus the results presented can stimulate further work on the polarized spectra of hydrocarbons. A systematic study of alkyl chain properties and phase behavior of intercalates in ilerite layers as a function of surface coverage, temperature and relative humidity will be given in a subsequent paper.

Materials and methods

Materials

The layered metal silicate hydrate ilerite was synthesized using hydrothermal procedures based on those described in Ref. [22] Dissolved sodium hydroxide (NaOH) was added slowly (15 min) under vigorous stirring to diluted colloidal silica sol (about 15 wt% SiO_2) to yield a reaction mixture of $4SiO_2/1Na_2O/35H_2O$ (mol/mol/mol). After homogenization by stirring (45 min) the mixture was filled into stainless-steel autoclaves and heated (100 °C) for 21 days. The product was separated by filtration, washed with de-ionized water and air-dried at room temperature to give a powder which consists of rectangular, plate-like single crystallites of $8.2SiO_2/1Na_2O/10.2H_2O$ composition (Fig. 1).

The cationic surfactant dodecyltrimethylammoniumbromide (DTAB) was intercalated by ion-exchange at room temperature. After suspending ilerite powder in deionized water the surfactant solution was added to yield final ilerite and DTAB concentrations of 0.1 g/l and 5.59×10^{-2} mol/l, resp. The suspension was stirred and after 4 h the product was separated and air dried to prevent secondary aggregation of the crystallites. The weight fraction of the intercalated surfactant amounts to $w_s \approx 0.35$. Micrographs of the product show essentially identical platelets when compared with the pure ilerite microcrystals (not shown).

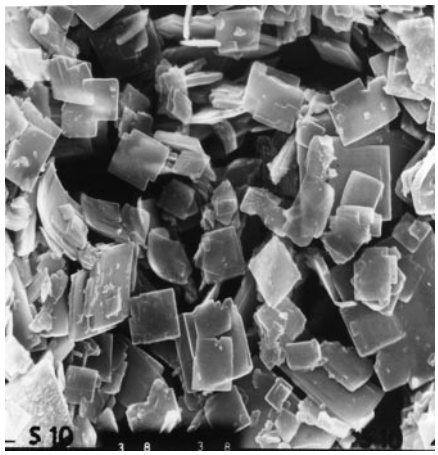

Fig. 1 Electron micrographs of ilerite crystallites which constitute plate-like single particles of about ($\sim 5 \times 5 \times 0.2$) μm dimensions

Infrared dichroism investigations

Sample preparation and FTIR-measurements

Samples were prepared by smearing a small amount of wet ilerite powder uniformly on the surface of a ZnSe-attenuated total reflection (ATR) crystal (50×5 mm; face angle 45°). The sample was subsequently dried under a stream of nitrogen. The amount of material corresponds to an average thickness of the sample film > 100 μm exceeding the penetration depth of the electromagnetic waves. Samples of pure DTAB were prepared by spreading 100 μl of a methanolic stock solution (5 mM) on the ATR crystal and evaporating the solvent under N_2. The ATR crystal was mounted on a commercial horizontal Benchmark unit (Specac. U.K.) modified in order to realize a definite relative humidity (RH) and temperature at the crystal surface coated with the sample [24].

The Benchmark unit was placed into a BioRad FTS-60a Fourier transform infrared spectrometer (Digilab, MA) equipped with a wire grid polarizer. Each single channel spectrum was recorded with 128 scans at two perpendicular orientations of the polarizer, one parallel and one perpendicular with respect to the surface normal of the ATR crystal. The polarized absorbance spectra of

the sample $A_{\parallel}(\nu)$ and $A_{\perp}(\nu)$ were registered with a resolution of 2 cm^{-1} using the respective single channel spectra of the empty ATR crystal as background.

The samples were investigated in dependence on temperature T at a constant relative humidity of RH = $90 \pm 2\%$ and $50 \pm 2\%$ (ilerite + DTAB) and $60 \pm 2\%$ (DTAB). The temperature was increased in steps of 1 K. Before measurement the sample was allowed to equilibrate for at least 10 min after reaching the prescribed T in each step resulting in an effective heating rate of 1.5 K/h. In special cases the samples were studied by means of variable RH in steps of 3% at constant temperature.

Determination of the infrared order parameter

The order parameter of an IR active transition moment, S_{IR}, is defined as

$$S_{IR} = \tfrac{1}{2}\langle 3\cos^2\theta_{\mu} - 1\rangle \quad (1)$$

with θ_{μ}, the angle enclosed by unit vectors parallel to an individual transition moment, **μ**, and the normal of the crystal surface **n**. The angular bracket denotes ensemble averaging over all absorbing transition moments in the sample, S_{IR} can be calculated from the dichroic ratio, R, of the corresponding absorption band by means of [25]

$$S_{IR} = \frac{R - K_1}{R + K_2} \quad \text{with} \quad R \equiv \frac{A_{\parallel}}{A_{\perp}} . \quad (2)$$

The polarized absorbances, $A_{\parallel}$ and $A_{\perp}$, are evaluated from $A_{\parallel}(\nu)$ and $A_{\perp}(\nu)$ by integration of the respective absorption bands after baseline correction (see below). In some cases Gaussian functions are fitted to the experimental spectra to separate overlapping bands. The constants $K_1 = 2$ and $K_2 = 2.55$ are calculated on the basis of the formulae given in Ref. [25] (see also [20]) for the electric field amplitudes in the rarer medium the thickness of which exceeds the penetration depth of the electromagnetic waves

$$K_1 = \frac{2\sin^2\omega - n_{21}^2}{(1 + n_{21}^2)\sin^2\omega - n_{21}^2} \quad \text{and}$$

$$K_2 = \frac{\sin^2\omega + n_{21}^2}{(1 + n_{21}^2)\sin^2\omega - n_{21}^2} ,$$

using an angle of incidence of $\omega = 45°$ and the ratio of the refractive indices of the sample and of the ZnSe crystal, $n_{21} \equiv n_{sample}/n_{ZnSe} = 0.58$ ($n_{ZnSe} = 2.44$ [26]). The treatment of the silicate layers with intercalated DTAB as an optically homogeneous medium with $n_{sample} = 1.42$ is justified by the very similar refractive indices of silicate glass ($n_{SiO} = 1.42$ at $\lambda = 3\ \mu m$ [26]) and of hydrocarbons ($n_{hc} = 1.41 \pm 0.01$ [27]).

For the estimation of the mean angle between the transition moment and the surface normal we used the approximation (cf. Eq. (1))

$$\langle\theta_{\mu}\rangle \approx \arccos\left(\sqrt{\tfrac{1}{3}(2S_{IR} + 1)}\right) . \quad (3)$$

Results

Orientation of the ilerite microcrystals

The polarized IR spectra of pure ilerite powder without intercalated surfactant (Fig. 2) show a series of five well-resolved, intense absorption bands at 1223 cm^{-1} ($S_{IR} > 0.9$), 1064 cm^{-1} (>0.7). 1036 cm^{-1} (< -0.45), 821 cm^{-1} (>0.7) and 784 cm^{-1} (< -0.4). The corresponding IR-order parameters given in the parentheses indicate that the IR active transition moments of the silica–oxygen network are oriented either strictly parallel or strictly perpendicular with respect to the normal of the ATR surface. Note, that $S_{IR} > 0.7$ corresponds to a dichroic ratio $R > 12$ where $A_{\parallel}$ exceeds $A_{\perp}$ by more than an order of magnitude and therefore the corresponding absorption band can be assumed to be strongly $\parallel$ polarized within the limits of experimental error ($\Delta S_{IR} \approx \pm 0.2$ at $S > 0.7$).

Metal silicate hydrates are built up by $Si(OSi\equiv)_3O^-$ and $Si(OSi\equiv)_4$ tetrahedra which are linked to each other to form two-dimensional layers [28]. The general features of vibrational spectra of layered silicates can be qualitatively interpreted in terms of a silica–oxygen network of ideal or distorted hexagonal symmetry which is composed of elementary units of the type $O_3Si–O–SiO_3$ [9] or (Si_nO_m) [29]. These analyses indicate Si–O lattice vibrations whose transition dipoles are oriented either parallel or perpendicular with respect to the normal of the silicate

Fig. 2 Polarized absorbance spectra, $A_{\parallel}(\nu)$ (solid line) and $A_{\perp}(\nu)$ (dotted line), of pure ilerite microcrystals spread on the ATR-surface

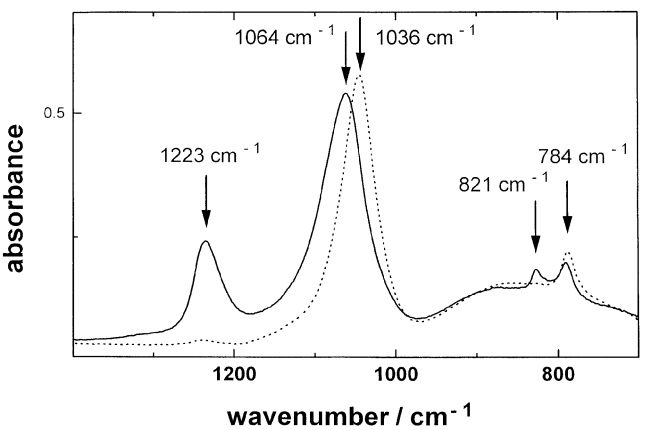

layers. This result in combination with the finding of the exclusively parallel or perpendicularly polarized absorption bands of ilerite gives indication that the normal of the silicate layers coincides with that of the ATR-surface, or in other words, the plate-like ilerite aligns strictly parallel on the crystal surface. The assignment of the different Si–O lattice modes of ilerite will be given elsewhere (in preparation).

The use of a Ge ATR crystal yields identical results. We suggest that the macroscopic orientation of the microcrystals is not the result of a specific interaction between ilerite and the ATR crystal but seems to be caused by sterical factors. The wetting and subsequent drying of the powder obviously promotes the sedimentation and/or cohesion of the platelets parallel to the plane support. Note that the exponentially decaying amplitude of the IR radiation samples the first 5–50 layers nearest to the crystal surface. Dry ilerite powder which is scattered about the crystal surface gives rise to weak IR absorbance because of poor optical contact.

To quantify the effect of nonparallel oriented platelets on S_{IR} let us introduce the unit vector **d** pointing along the normal of the surface of a microcrystal in addition to **n** and **μ** which are defined in the previous section. One can assume that the probability distribution for orientations of **d** around **n** is of cylindrical symmetry, and thus depends only on the angle $\delta(\mathbf{nd})$ which is enclosed between both vectors. If the relative orientations of **d**, **n** and **μ** are independent of each other then S_{IR} can be written as the product

$$S_{IR} = S_{\mathbf{d}} \cdot S_{\boldsymbol{\mu}} , \tag{4}$$

where $S_{\mathbf{d}}$ and $S_{\boldsymbol{\mu}}$ are defined analogously as S_{IR} (cf. Eq. (1)) but using $\delta(\mathbf{nd})$ and the angle $\delta(\mathbf{d\mu})$ which is enclosed between **d** and **μ** instead of $\theta_{\mu} \equiv \delta(\mathbf{n\mu})$, respectively. Consequently, $S_{\mathbf{d}}$ represents a measure of the degree of macroscopic ordering of the platelets with respect to the ATR surface whereas $S_{\boldsymbol{\mu}}$ quantifies the mean orientation of the transition moment within the microcrystal. For the transition moments of the lattice modes we assumed $S_{\mu} = 1$ (or $S_{\mu} = -0.5$). The measured value of the absorption band at $1223\,\mathrm{cm}^{-1}$, $S_{IR} > 0.9$, yields consequently $S_{\mathbf{d}} > 0.9$ which corresponds to a mean angle of $\langle\delta(\mathbf{nd})\rangle < 15^{\circ}$ (cf. Eq. (3)). For the estimation of the orientations of molecules intercalated between the silicate layers we can use $S_{\mathbf{d}} = 0.95$ to a good approximation (see below).

Methyl and methylene absorption bands of DTAB

The linear dichroism of the characteristic absorption bands of pure ilerite and of ilerite with intercalated DTAB is essentially identical. This fact indicates a similar alignment of the ilerite platelets on the ATR surface in both cases. The macroscopic orientation of the microcrystals offers the possibility to study the molecular arrangement of the surfactant which is intercalated between the host matrix by means of IR spectroscopy.

The long-chain alkylammonium ion DTAB gives rise to a number of absorption bands which originate from vibrations of the methyl and methylene groups of the alkyl chains. The C–H stretching region of DTAB is dominated by two strong features which can be assigned to the symmetric and antisymmetric methylene stretching vibrations (cf. Fig. 3). The polarized absorbance spectra $A_{\parallel}(\nu)$ and $A_{\perp}(\nu)$ give first indication of the molecular ordering within the sample. The spectrum of the dichroic ratio, $R(\nu) = A_{\parallel}(\nu)/A_{\perp}(\nu)$, shown in the upper part of Fig. 3 is well suited to detect subtle differences between the polarization of the respective absorption bands. It reveals a significantly smaller dichroic ratio of the $\nu_{as}(CH_2)$ band at $T = 20\,^{\circ}\mathrm{C}$ when compared with that of the $\nu_s(CH_2)$ mode.

Fig. 3 Polarized infrared spectra, $A_{\parallel}(\nu)$ (solid line, below) and $A_{\perp}(\nu)$ (dotted line, below) of the C–H stretching region of DTAB intercalated between ilerite layers at $T = 20\,^{\circ}\mathrm{C}$. The corresponding dichroism spectrum $R(\nu) = A_{\parallel}(\nu)/A_{\perp}(\nu)$ is depicted in the upper part together with that obtained at $T = 50\,^{\circ}\mathrm{C}$ (crosses). The gray areas illustrate the integrated absorbances $A_{\perp}$ of the symmetric and antisymmetric CH_2 stretching bands which are used for the determination of the IR order parameters. The $A_{\parallel}$s were calculated by integration of $A_{\perp}(\nu)$ over the same spectral range. The spectra are corrected using a linear baseline drawn between 3000 and 2800 cm^{-1}

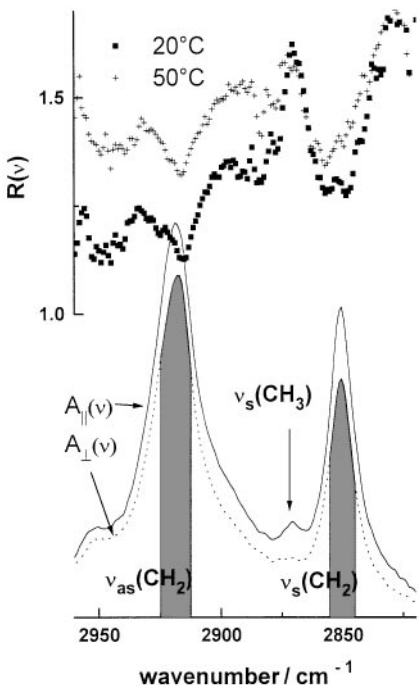

Note that the spectral overlap of the $\nu_{as}(CH_2)$ band with the broad Fermi resonance band cannot explain the observed effect for the following reasons: (i) The Fermi resonance involves the interaction between the symmetric CH_2 stretching fundamental with appropriate binary combinations of the methylene bending dispersion [13]. Hence, the corresponding absorption band is expected to possess the same dichroism as the $\nu_s(CH_2)$ mode. Consequently, the spectral overlap with the $\nu_{as}(CH_2)$ band would more likely tend to compensate dichroic differences between both methylene stretching bands than to cause it. Exactly this tendency can be observed in the $R(\nu)$ spectrum in the spectral range corresponding to the flanks of the $\nu_{as}(CH_2)$ band where the fractional contribution of the underlying Fermi resonance band increases. (ii) The chosen baseline (see legend of Fig. 3) subtracts the residual absorbance of the $\nu_{13}(OH)$ band of water from the C–H region. Specific spectral features in this range are not considered. Typically this baseline is expected to underestimate the dichroism of the methylene stretching bands. The apparent difference between the dichroism of both bands should be interpreted as a lower limit of an effect which is possibly slightly more pronounced. (iii) At higher temperatures ($T = 50\,^{\circ}C$, cf. Fig. 3) the difference between the dichroism of both methylene bands vanishes (for the interpretation see below). It seems unlikely that the obscuring effect of Fermi resonance or of other systematic error sources, if present, can modify the spectral pattern in this manner. (iv) The dichroic difference discussed is much more pronounced in films of pure DTAB (see below) where it exceeds the significance level clearly.

To minimize errors we calculate the integral absorbance of the CH_2 stretching bands over the spectral ranges which correspond to an absorbance exceeding 60% of the respective maximum absorbance (see Fig. 3 for illustration). The IR order parameters, $S_{IR}(\nu_s(CH_2))$ and $S_{IR}(\nu_{as}(CH_2))$, are shown in Fig. 4 as a function of temperature. At $T < 40\,^{\circ}C$ $S_{IR}(\nu_{as}(CH_2))$ is significantly smaller (more negative) than $S_{IR}(\nu_s(CH_2))$ whereas at $T > 45\,^{\circ}C$ both parameters adopt similar values. The centers of gravity of the corresponding absorption bands, $COG(\nu_s(CH_2))$ and $COG(\nu_{as}(CH_2))$, increase monotonically upon heating showing a sigmoidal step centered around $40\,^{\circ}C$ (Fig. 4). This behavior is typically observed at the melting transition of *n*-alkanes and of amphiphiles where the hydrocarbon chains transform from a solid to a fluid-like state (see, e.g., [14, 17]). Note, that in contrast to the IR order parameters the COGs of both CH_2 stretching modes change nearly perfectly parallel to each other. The finding provides an additional argument in favor of the assumption that the origin of the different S_{IR} at $T < 40\,^{\circ}C$ should be sought in effects of molecular orientation and not in systematic errors because, e.g., overlapping bands are expected to obscure the COGs of the symmetric and antisymmetric modes in a different fashion.

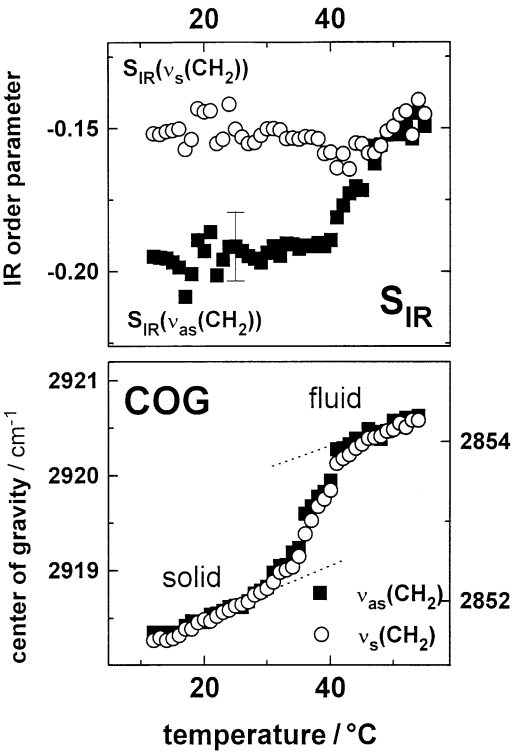

Fig. 4 Infrared order parameter (S_{IR}) and center of gravity (COG) of the antisymmetric (black squares) and symmetric (open circles) methylene stretching vibration of DTAB intercalated between ilerite layers at RH = 90% as a function of temperature. The left and right axes in the lower part correspond to $COG(\nu_{as}(CH_2))$ and $COG(\nu_s(CH_2))$ resp. In order to eliminate dichroic effects on the COG it was determined from the superposition of the polarized spectra $A(\nu) = A_{\parallel}(\nu) + K_2 \cdot A_{\perp}(\nu)$. The representative error bar corresponds to the standard error of five independent preparations

Pure DTAB reveals similar properties when heated at RH = 60% (Fig. 5). In contrast to the intercalated surfactant the IR order parameters of the pure surfactant adopt values near zero at temperatures above the phase transition temperature. Obviously the macroscopic molecular order disappears completely after melting.

Figure 6 shows the polarized spectra of pure DTAB in the range 1500–1450 cm^{-1}. It is characterized by overlapping absorption bands originating from the methylene bending vibration of the alkyl chains, $\delta(CH_2)$, and from two antisymmetric methyl bending modes of the trimethylammonium groups, $\delta^{A}_{as}(CH_3)^{TA}$ and $\delta^{E}_{as}(CH_3)^{TA}$ [20] (see also Table 1). The extinction coefficient of the latter vibrations is obviously much higher than that of the $\delta(CH_2)$ mode probably because of the influence of the adjacent heteroatom (N^+). The $\delta(CH_2)$ vibration splits into two clearly resolved component bands which are

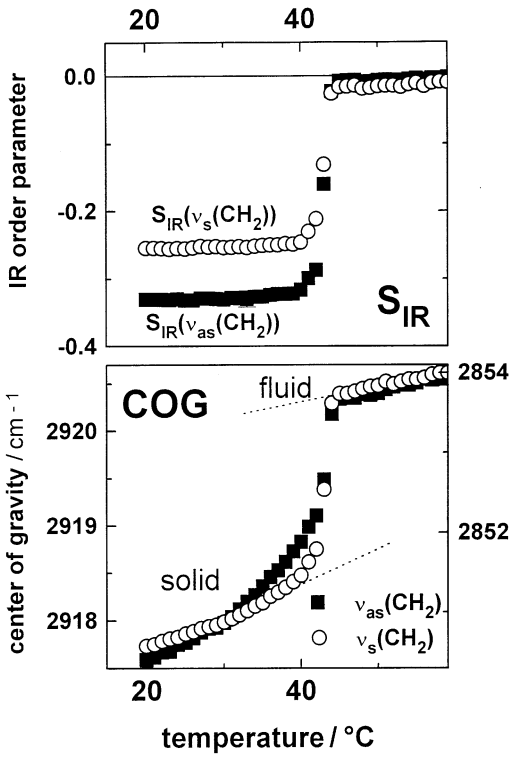

Fig. 5 Infrared order parameter (S_{IR}) and center of gravity (COG) of the antisymmetric (black squares) and symmetric (open circles) methylene stretching vibration of pure DTAB spread on the ATR surface at RH = 60% as a function of temperature. The left and right axes in the lower part correspond to COG($\nu_{as}(CH_2)$) and COG($\nu_s(CH_2)$), resp. Note that the S_{IR} axes in Figs. 4 and 5 are differently scaled

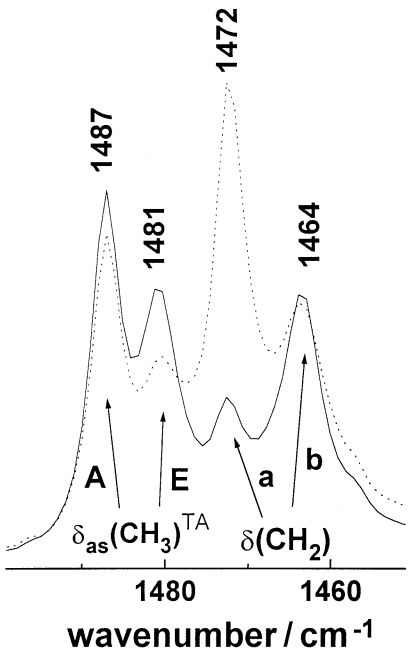

Fig. 6 Polarized infrared spectra, $A_{\parallel}(\nu)$ (solid line) and $2xA_{\perp}(\nu)$ (dotted line), of the methyl and methylene bending vibrations of pure DTAB at $T = 20\,^{\circ}C$. Band assignments are given within the figure and in the text

polarized differently. This effect arises typically if alkyl chains in the extended *all-trans* conformation pack into a crystalline subcell where the reorientational motions about the chain axes are completely damped. In this case the $\delta(CH_2)$ vibrations of laterally adjoining chains couple and split into an in- and out-of-phase component the transition dipoles of which point along the crystalline *a*- and *b*-axis, resp. [12, 30]. Note that the splitting of the $\delta(CH_2)$ band is paralleled by the splitting of the CH_2 rocking band appearing as a doublet with maxima at 729 and 719 cm^{-1} in crystalline DTAB (not shown).

The integral polarized absorbances of the $\delta(CH_2)$ subbands are determined from the areas of Gaussian functions

Table 1 Positions, fractional intensities[b], and infrared order parameters of the methylene and methyl bending bands of DTAB shown in Figs. 6 and 7[a]. The assignments of the bands are given in the first column

Vibration	Symbol	Property[c]	Pure	Intercalated[a]	
			$T = 20\,^{\circ}C$	$T = 20\,^{\circ}C$	$T = 55\,^{\circ}C$
Methylene bending	$\delta(CH_2)$	maximum cm^{-1}	1464/1472	1466/1472	1467
		fractional intensities[b]	0.53/0.47	0.52/0.48	–
		S_{IR}	0.01/−0.40	−0.16/−0.25	−0.18
Methyl bending	$\delta_{as}^{E}(CH_3)^{TA}$	maximum cm^{-1}	1481	1481	1479
E mode		S_{IR}	0.03	0.08	−0.01
Methyl bending	$\delta_{as}^{A}(CH_3)^{TA}$	maximum cm^{-1}	1487	1491	1491
A_1 mode		S_{IR}	0.13	−0.22	−0.17

[a] Four ($T = 20\,^{\circ}C$) or three ($T = 55\,^{\circ}C$) Gaussian functions are fitted to the spectra as illustrated in Fig. 7. Note that the fits are coupled for each pair of polarized spectra, $A_{\parallel}(\nu)$ and $A_{\perp}(\nu)$, by the condition of equal positions and widths of the corresponding Gaussian functions.
[b] $f^a = A^a/(A^b + A^a)$ and $f^b = 1 - f^a$, with $A^i = A_{\parallel}^i + K_2 \cdot A_{\perp}^i$, $i = a, b$: $A_{\parallel}^i$ and $A_{\perp}^i$ are the areas of the respective Gaussian functions.
[c] SE: ± 0.02 (S_{IR}): ± 0.5 cm (maximum), ± 0.02 (fractional intensity).

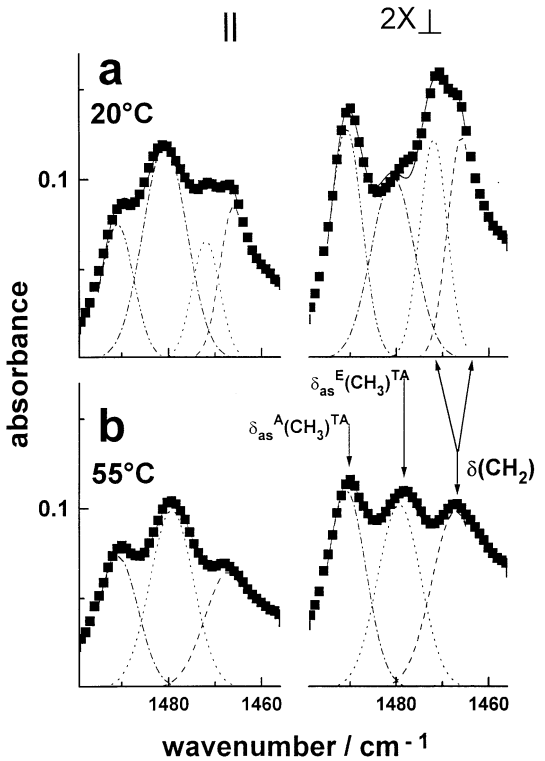

Fig. 7 Polarized infrared spectra. $A_{\parallel}(v)$ (*a*, left) and $2 \times A_{\perp}(v)$ (*b*, right), of the methyl and methylene bending vibrations of DTAB intercalated between ilerite layers at $T = 20\,^{\circ}\mathrm{C}$ (above) and $55\,^{\circ}\mathrm{C}$ (below). Experimental data are shown by symbols and Gaussian fit functions by lines. Note that the spectrum of pure ilerite is smooth in the corresponding range. It has been subtracted prior to band fitting

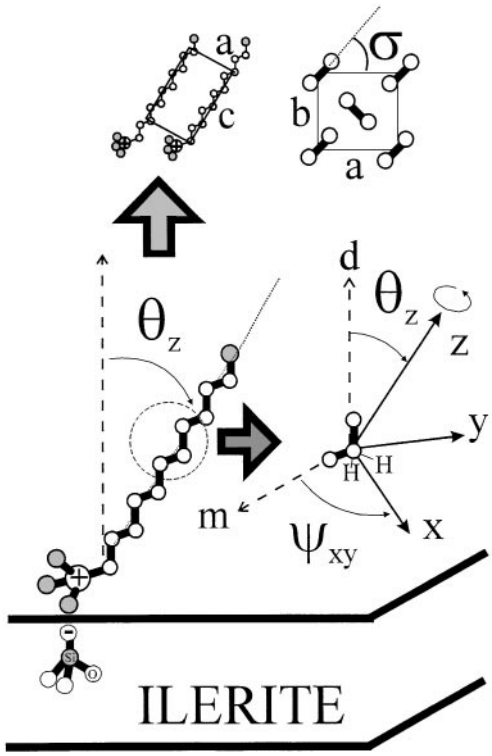

Fig. 8 Schematic representation of the alkyl chain orientation of DTAB intercalated between ilerite layers. Only one-half of the silicate layer is shown. The right part enlarges the molecular frame fixed to a methylene group. **d** denotes the normal of the silicate layer and **m** is the normal of the *z***d**-plane pointing parallel to the layer. The axis and setting angle of the orthorhombic subcell are given in the upper part

which are fitted to the polarized spectra. They yield the corresponding IR order parameters, S_{IR}, and the fractional absorbances of the subbands, f^{a} and f^{b} (see Table 1). These values give rise to the setting angle, $\sigma = \arctan\{(f^{b}/f^{a})^{0.5}\}$, which enclose the polymethylene planes with the *a*-axis of the subcell [12] (see Fig. 8 for illustration). The almost equal fractional absorbances yield $\sigma = (47 \pm 3)^{\circ}$, the setting angle of an orthorhombic perpendicular subcell, $O_{\perp}$.

DTAB intercalated in ilerite reveals similar spectral features in the 1450–1500 cm^{-1} region as the pure surfactant (Fig. 7 and Table 1). The existence of a $\delta(CH_2)$ doublet is confirmed by the splitting of the rocking band becoming evident in the polarized spectra at 719–726 cm^{-1} (not shown). The low-frequency splitting component $\delta(CH_2)^{b}$ is, however shifted to higher wavenumbers by $\sim 2\,\mathrm{cm}^{-1}$ when compared with the $\delta(CH_2)^{b}$ mode of pure DTAB. Changes of the frequency difference between the subbands can be interpreted in the framework of the coupled oscillator model which predicts a quantitative relation between the size of crystalline $O_{\perp}$-domains and the normalized band splitting, $R_s = \Delta\nu/\Delta\nu_0$, namely

$$N_1 = \frac{\pi}{\sqrt{2(1 - R_s)}} - 1 \quad \text{and} \quad N_2 = \left(\frac{\pi}{\arccos R_s} - 1\right)^2$$

for one-dimensional, linear and two-dimensional, square domains, resp. [30]. Using for the maximum splitting, $\Delta\nu_0$, the frequency difference between the subbands in pure DTAB one obtains for the intercalated surfactant with $R_s \approx 0.75\, N_1 \approx 3.5$ and $N_2 \approx 11$. In other words, the regular packing of the alkyl chains between the host layers appears to be perturbed by defects which laterally decouple the methylene bending modes of adjacent molecules. On the average ~ 3.5 alkyl chains can be thought to form an undisturbed linear and ~ 11 chains an undisturbed compact square $O_{\perp}$ domain to account for the observed splitting. Note that a reduced splitting of the $\delta(CH_2)$ band of $O_{\perp}$ structures was observed in assemblies of amphiphilic molecules as, e.g., lipid membranes in the

solid state [24, 31, 32]. Interestingly the width of the b component band of $\sim 7\,\mathrm{cm}^{-1}$ remains nearly constant for pure and intercalated DTAB. This value corresponds to a relatively narrow distribution of setting angles in both systems [32]. In the fluid phase ($T = 55\,^{\circ}\mathrm{C}$) the $\delta(CH_2)$ component bands merge into a broad singlet indicating the disappearance of the transversal ordering of the alkyl chains.

Summarizing the experimental findings, we conclude from the crystal field splitting of the $\delta(CH_2)$ vibration and from the typical sigmoidal upwards shift of the COGs of the CH_2 stretching modes that DTAB intercalated between ilerite layers upon heating undergoes a phase transition from a solid state where the alkyl chains are arranged in a crystalline lattice to a fluid state which is characterized by molten chains. In contrast to pure DTAB the intercalated surfactant maintains a lamellar arrangement in the fluid state owing to the constraints of the host matrix.

Discussion

IR order parameters and the tilt of the alkyl chains

To characterize the molecular order of the alkyl chains it will be appropriate to fix cartesian frames of reference $\{x, y, z\}$ to each methylene group with x bisecting the angle included between the C–H bonds and z intersecting the centers of subsequent C–C bonds (see, Fig. 8). The transition moments of the symmetric and antisymmetric CH_2 stretching modes in an isolated methylene group point along the molecular x- and y-axes, resp., giving rise to the IR order parameters $S_x \equiv S_{IR}(\nu_s(CH_2))$ and $S_y \equiv S_{IR}(\nu_{as}(CH_2))$. The equations [33, 34]

$$S_z \equiv \tfrac{1}{2}(3\langle\cos^2\theta_z\rangle - 1) = -(S_x + S_y)\,, \tag{5}$$

$$D_{xy} \equiv \tfrac{3}{2}\langle\sin^2\theta_z\cdot\cos^2\psi_{xy}\rangle = (S_x - S_y)\,, \tag{6}$$

define the tilt order parameter S_z and the transverse order parameter, D_{xy} also called dispersion. It characterizes the biaxiality of the molecular arrangement, i.e., the degree of rotational asymmetry of the molecular orientations about the molecular z-axis. The tilt angle θ_z and the azimuthal angle ψ_{xy} are defined in Fig. 5. Note, that Eqs. (5) and (6) hold for cylindrical symmetric distributions of the molecular z-axis around the optical axis **n**. This condition is satisfied in the present powder sample because the existence of macroscopical ordering of any in-plane direction of the silicate layers can be excluded.

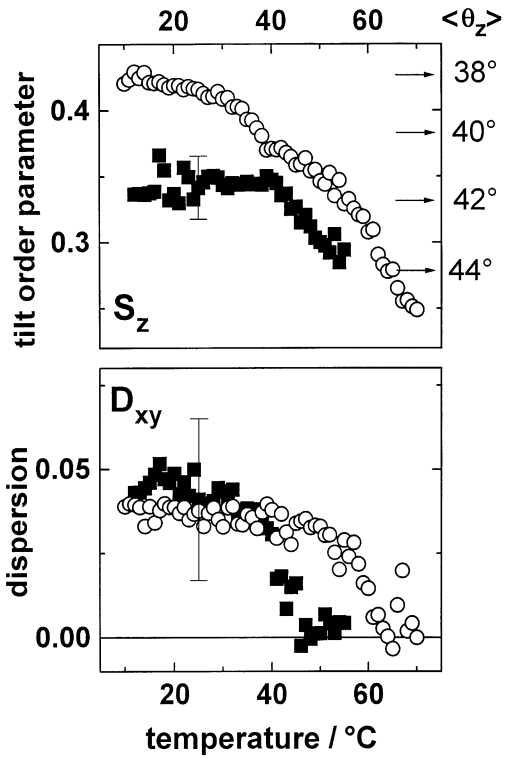

Fig. 9 Tilt order parameter (S_z) and dispersion (D_{xy}) of the alkyl chains of DTAB intercalated between ilerite layers at RH = 90% (solid squares) and 50% (open circles) as a function of temperature. S_z and D_{xy} are calculated by means of Eqs. (5) and (6) using $S_{IR}(\nu_s(CH_2))$ and $S_{IR}(\nu_{as}(CH_2))$. The right scale of the upper part gives the apparent mean tilt angles $\langle\theta_z\rangle$

S_z represents a measure of the mean orientation of the fiber axes of the alkyl chains with respect to the normal of the silicate layers **d**. In the crystalline state of intercalated DTAB it adopts values of ~ 0.34 at RH = 90% (Fig. 9). This value corresponds to an apparent mean tilt angle of the long axes of the *all-trans* extended alkyl chains of $\langle\theta_z\rangle \approx 42^{\circ}$ (cf. Eq. (3)). If one takes into account the non-perfect alignment of the ilerite microcrystals by using Eq. (4) and $S_d = 0.95$ then $\langle\theta_z\rangle$ increases slightly by less than 0.8°. This correction is clearly smaller than the standard error ($\pm 2^{\circ}$) and therefore imperfections of the macroscopic orientation can be neglected to a good approximation. Although S_z drops distinctly at the phase transition its value significantly deviates from zero also in the fluid phase indicating a considerable residual ordering of the alkyl chains in contrast to pure DTAB. The dispersion, D_{xy}, decreases from ~ 0.05 to zero upon transformation from the solid to the fluid state. This finding indicates that the fixed arrangement of the polymethylene planes vanishes at the phase transition owing to the onset of reorientations of the DTAB molecules about their long

axes. The interpretation is confirmed by the fact that the disappearance of the crystal field splitting of the CH_2 bending mode at the phase transformation correlates with this typical change of D_{xy}.

In a crystalline $O_\perp$-lattice the transition moments of the $\delta(CH_2)^a$ and $\delta(CH_2)^b$ bands are directed parallel to the *a*- and *b*-axes of the subcell, resp., as predicted theoretically [12, 30] and confirmed by the polarized IR spectra of crystalline *n*-alkanes [35]. Owing to the orthogonality of the *a*-, *b*- and *c*-axes Eqs. (5) and (6) remain valid if one substitutes S_x and S_y by $S_b \equiv S_{IR}(\delta(CH_2)^b)$ and $S_a \equiv S_{IR}(\delta(CH_2)^a)$, resp. Using the respective values given in Table 1 ($T = 20\,^\circ C$) one obtains the tilt order parameter $S_c = 0.41 \pm 0.04$ and the dispersion $D_{ab} = 0.10 \pm 0.04$. S_c refers to the angle θ_c, which is enclosed between the crystalline *c*-axis and the layer normal Eq. (3) yields the apparent tilt angle of the *c*-axis $\langle\theta_c\rangle \approx 39^\circ$. The *c*-axis of the subcell and the long axes of the alkyl chains are directed parallel in a perfect crystalline lattice of *all-trans* alkyl chains. Consequently S_c and S_z are expected to be equal. The slightly smaller value of $S_c = 0.34 \pm 0.03$ in comparison with S_c can be attributed (i) to small tumbling motions of the chain axes about their mean orientation and, (ii) to small variations of the torsion angles between adjacent methylene groups (librotorsional motions) leading to deviations from the antiperiplanar conformation of the methylene units [19].

The temperature dependence of the order parameters measured at the reduced humidity RH = 50% indicates the shift of the chain melting transition temperature up to about 60 °C (Fig. 9). This behavior is typically found in amphiphilic assemblies at a limited degree of hydration and can be understood qualitatively in terms of increasing vapor pressure acting on the system [24, 36]. Interestingly, dehydration causes an increased conformational order of the alkyl chains accompanied with a decreased tilt angle of the chain axes but almost no changes of the transverse order parameter.

The significance of this finding has been proven by the RH scans of independent samples which are performed at constant temperature (Fig. 10a). Whereas the intercalated surfactant exists in the crystalline state throughout the whole RH-range investigated (5–98%), the pure DTAB undergoes the melting transition at RH = 68–70% as indicated by the drastic drop of the corresponding dispersion. A similar solid/fluid transition was observed upon hydration of monolayers of hexadecyltrimethylammonium bromide (CTAB) assembled on a solid support (mica) [37]. The authors suggested that water adsorption to the polar moieties of the surfactant affects the system in two ways: First, a hydration layer forms at the solid/headgroup interface which reduces the monolayer/substrate adhesion. Second, the hydrated headgroups move farther apart laterally, and thus the inter-head-group and inter-chain cohesion loosen. The second effect can be thought to be suppressed to a high degree in ilerite because of the tight binding of the trimethylammonium groups to the charged groups of the host layers. As a result the silicate layers stabilize the solid phase of DTAB in agreement with the observations.

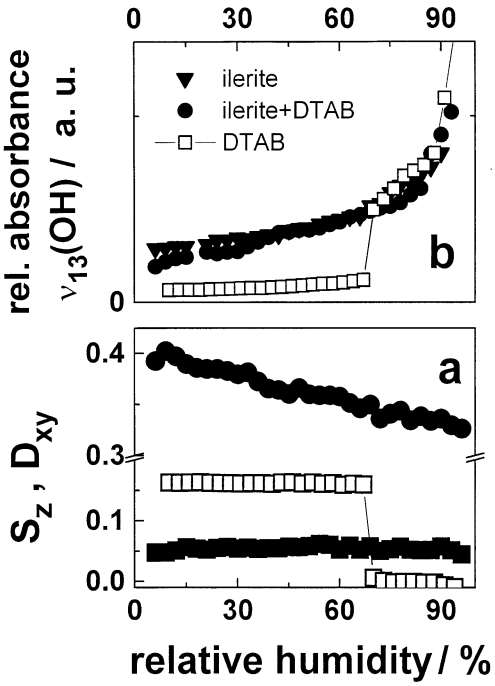

Fig. 10 (a) Tilt order parameter (S_z, solid circles) and dispersion (D_{xy}, solid squares) of the alkyl chains of DTAB intercalated between ilerite layers at $T = 25\,^\circ C$ as a function of the relative humidity (RH). The open squares correspond to the dispersion, D_{xy}, of pure DTAB at 25 °C. (b) Relative absorbance, A_{rel}, of the ν_{13}(OH) band of water sorbed onto pure ilerite (down triangles), onto ilerite + DTAB (solid circles) and onto pure DTAB (open squares) as a function of RH. A_{rel} was calculated using the integral $A(\nu_{13}) = \int\{A_\parallel(\nu) + K_2 \cdot A_\perp(\nu)\}\,d\nu$ taken in the range 3700–3000 cm^{-1}. It was normalized to the integrated intensity of the CH_2 stretching bands of DTAB (pure and intercalated) measured at RH = 10%, i.e., $A_{rel} = A(\nu_{13})/A(\nu CH_2)_{RH=10\%}$. In the case of pure ilerite $A(\nu_{13})$ was normalized to the integrated absorbance of the SiO lattice mode centered at 1064 cm^{-1} by $A_{rel} = (A(\nu_{13})/A(1064)) \cdot \{A(1064)/A(\nu CH_2)_{RH=10\%}\}_{DTAB+ilerite}$ where the integral absorbances in parentheses $\{\ldots\}$ correspond to DTAB + ilerite

The integrated absorbance of the OH stretching region of water, A_{rel}(OH), is well suited as a relative measure of the amount of water sorbed to the samples [24]. Figure 10b depicts A_{rel}(OH) for pure ilerite, for pure DTAB and for ilerite with intercalated DTAB. Note that the data can be compared directly with each other because A_{rel}(OH) has been normalized using the intergrated absorbances of the CH_2 stretching region and/or of a SiO lattice mode as internal standards (see legend of Fig. 10).

This analysis shows that pure DTAB is nearly anhydrous in the crystalline state but it rapidly adsorbs water upon melting. The phase transition is completely reversible. No significant differences of the hydration of pure ilerite and of ilerite + DTAB can be detected. Obviously the sorption of water to ilerite is not affected by the crystalline DTAB when intercalated between the host layers. We suggest that besides specific hydration sites capillary condensation can significantly contribute to the hydration properties of the powder samples especially at RH values near 100%.

The IR order parameters of the CH_3, bending vibrations listed in Table 1 reveal insight into the mean orientation of the trimethylammonium groups. If one assumes that the transition moments of the A_1 mode points along the C–N bond [20] then the negative values of $S_{IR}(\delta^{A}_{as}(CH_3)^{TA})$ suggest its preferential in-plane orientation with respect to the silicate layer. $S_{IR}(\delta^{A}_{as}(CH_3)^{TA})$ varies only slightly at the solid/fluid phase transition. We conclude that the lamellar order of the molten alkyl chains of intercalated DTAB is caused by the strong coulombic interactions between the $Si–O^-$ groups of ilerite and the $C–N^+–(CH_3)_3$ groups which fix their orientation and position also in the fluid state of the alkyl chains. The $S_{IR}(\delta^{E}_{as}(CH_3)^{TA})$ values around zero (Table 1) are in qualitative agreement with $S_{IR}(\delta^{A}_{as}(CH_3)^{TA}) < 0$ if one considers that the transition moment of the *E*-mode points perpendicularly with respect to that of the A_1 mode. A more detailed picture of the orientation and conformation of the polar part of DTAB will be given separately analyzing in addition the absorption bands of the C–N stretching modes located in the spectral range 1000–900 cm^{-1} (in preparation).

Dimensions of the ilerite layers before and after intercalation of DTAB

The interpretation of the IR linear dichroism data in terms of the tilt angle of the alkyl chains is confirmed by the results of preliminary X-ray measurements on hydrated ilerite with and without intercalated DTAB (see [38] for details of the measurements). The analysis of the diffraction pattern gives rise to a basal spacing which increases from $d_I = 1.1$ nm (pure hydrated ilerite, $T = 20\,^{\circ}C$. RH $\approx 100\%$, see also [23]) up to $d_{S+I} = 2.38$ nm after intercalation of DTAB ($T = 20\,^{\circ}C$, RH $\approx 100\%$, solid DTAB). It is reasonable to assume that the silica–oxygen network is not affected by the surfactant. Moreover, we found no significant changes of the amount of sorbed water when comparing ilerite before and after intercalation of DTAB (see above). If one neglects in addition the ion exchange then the increment of the repeat distance can be attributed to the intercalated molecules which arrange in between the host layers. The interlayer separation is roughly given by $d_S = d_{S+I} - d_I \approx 1.28$ nm (see Fig. 11 for illustration). The length of a DTAB molecule in the extended *all-trans* configuration accounts to $L_S \approx 1.69$ nm when using standard bond lengths and angles for an estimation [39]. To fit into the gap between the ilerite layers the surfactant molecules must tilt by an angle of at least $\gamma_t = \arccos(d_S/L_S) \approx 41^{\circ}$ the value of which agrees fairly well with that obtained from the IR order parameters.

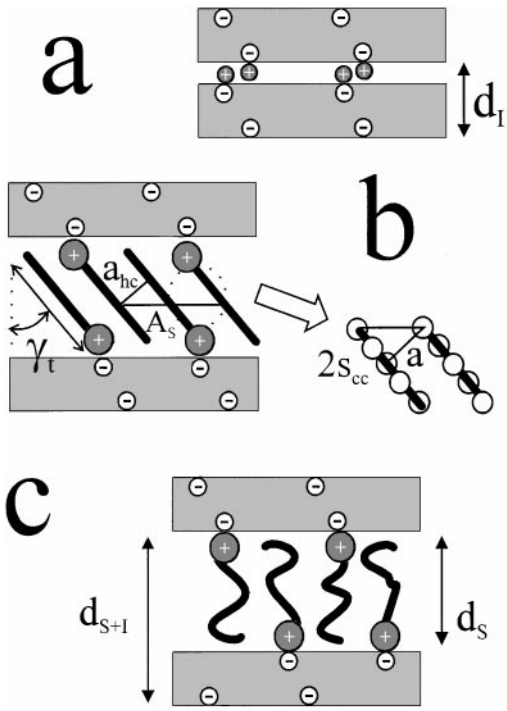

Fig. 11 Schematic representation of pure ilerite layers (a) and of ilerite layers with intercalated DTAB in the solid (b) and fluid (c) states. See text for explanations

The mean cross-sectional area per surfactant molecule in a plane parallel to the silicate layers can be estimated from the interlayer separation by

$$A_S = \frac{2 \cdot v_S}{d_S}. \tag{7}$$

The density of long-chain surfactants with frozen polymethylene chains is given to a good approximation by $\rho_s \approx 1$ g/cm^3 [39, 40]. This value yields the molecular volume of DTAB, $v_s \approx 0.38$ nm^3, and the area per molecule of $A_s \approx 0.58$ nm^2. In an $O_\perp$ subcell the cross section of the alkyl chains perpendicularly to the chain axes amounts

typically to $a_{hc} \approx 0.19\ nm^2$ [41]. If the area per molecule exceeds more than twice the cross section of the *all-trans* hydrocarbon chain then single-chained surfactants in the crystalline state often form lamellae where the molecules assemble in a head-to-tail fashion with interdigitated and tilted chains [41]. Exactly this situation i.e., $A_s > 2 \cdot a_{hc}$, applies to the geometric parameters obtained. The estimation of the tilt angle by $\cos \gamma_t = 2 \cdot a_{hc}/A_s$ [41] yields $\gamma_t \approx 49^\circ$ (see Fig. 11b).

Consequently, the tilt of the alkyl chain axes can be explained by the mismatch between the area per trimethylammonium group in the plane of the silicate layer on the one hand and the smaller cross section of the alkyl chains in the *all-trans* extended conformation on the other hand. The tilt realizes in this way a denser packing of the alkyl chains. Note that a similar situation is usually found in crystalline lamellar aggregates of long-chain surfactants such as lipids where the mismatch between the cross section of the polar headgroups and that of the polymethylene chains causes tilted phases [38, 42]. Also crystalline dodecylammonium bromide exhibits a monoclinic form where the molecules pack head-to-tail in single layers with the hydrocarbon chains tilted by 27° for similar reasons [43].

In contrast to assemblies of free surfactant molecules the area per DTAB intercalated in ilerite is determined by the distibution of charged $\equiv Si\text{–}O^-$ groups on the surface of the silicate layers. The mean area per anionic group in ilerite $A_{SiO^-} = 0.54\ nm^2$ [44] practically equals to $A_S \approx 0.58\ nm^2$ in view of the approximations made. This relation is expected if the cationic trimethylammonium groups of DTAB completely cover the anionic charges of ilerite. The actual value of A_S represents therefore the minimal area per DTAB and thus refers to the closest arrangement of the surfactant molecules in between the silicate layers.

Taking together we obtained indication by two independent methods that the frozen alkyl chains of DTAB tilt by an angle of $\theta_c \approx \theta_z \approx \gamma_t = 38\text{–}49^\circ$ to realize a dense packing within the gap between the silicate layers. Usually the tilt angle of crystalline polymethylene chains adopts discrete values which correspond to a stepwise, carbon-by-carbon, dislocation of one chain on the next [39] (see Fig. 11b for illustration). The possible tilt angles are roughly given by $\tan(90^\circ - \gamma_t'') \approx a/(n\, s_{CC})$ where $a \approx 0.49$ nm is the distance between adjacent CH_2 chains along the *a*-axis of the $O_\perp$ subcell and $s_{CC} \approx 0.1265$ nm refers to the projection of a CC bond onto the chain axis. For $n = 3$ and 4 one obtains 38° and 46°, respectively. We conclude that the alkyl chains of DTAB are dislocated by 3–4 carbons each to another to realize the tilt angle determined.

The basal spacing measured after the melting of the alkyl chains, $d_{S+I} = 2.71$ nm, corresponds to an increased interlayer separation of $d_S = 1.61$ nm. The lateral arrangement of the trimethylammonium groups can be assumed to remain almost unaffected by the phase transition owing to constraints which excert the charged groups of ilerite on the lateral distribuion of DTAB. In this case the increment of the interlayer spacing can be explained by a decrease of the density of the surfactant which is expected to amount to the ratio of the interlayer separations before and after melting, i.e., $1.28/1.61 = 0.8$. The density of *n*-alkanes and the density of polymethylene chains which are arranged in surfactant aggregates such as lipid bilayers is known to decrease upon melting by a factor of 0.78–0.85 [40] in reasonable agreement with the density change of DTAB deduced from the increase of the basal spacing of ilerite.

Conclusions

(i) Macroscopically oriented samples of silicate layers can be prepared very easily. The trivial but remarkable finding that the plate-like ilerite microcrystals align spontaneously parallel with respect to the ATR-surface enables the application of infrared dichroism measurements in order to study the orientation of molecules intercalated between the silicate layers.

(ii) The infrared order parameters of the intense symmetric and antisymmetric CH_2 stretching bands can be interpreted in terms of the tilt order parameter and the dispersion. The former yields the mean tilt angle of the alkyl chain axes whereas the latter can serve as an empirical measure of the freedom of the alkyl chains for rotations about their long axes. Owing to the relatively complex nature of the CH_2 stretching region of hydrocarbons [13] our interpretation of the IR order parameters in terms of S_z and D_{xy} represents a relative simple, preliminary approach. A comprehensive treatment of this problem is however impeded at present by the deficiency of dichroic data of the methylene stretching bands of hydrocarbon chains packed in several crystalline structures.

(iii) The dichroism of absorption bands originating from vibrations of the trimethylammonium groups gives insight into details of their orientation at the surfactant/silicate interface. The electrostatic interactions between the charged groups stabilize the crystalline state of DTAB and the lamellar ordering of the surfactant in the fluid phase when compared with the properties of pure DTAB.

(iv) The particular arrangement of the detergent can be modulated by temperature and/or relative humidity.

The latter fact indicates that the amphiphilic properties of the detergent are retained in the microconstrained state and thus, water obviously plays an important role for the physico-chemical properties of the system.

Acknowledgements We thank Dr. T. Gutberlet for stimulating discussion and the disposal of X-ray data. This work was supported by the Deutsche Forschungsgemeinschaft under Grant of SFB294.

References

1. Lagaly G, Beneke K (1991) Colloid Polym Sci 269:1198–1211
2. Beneke KBL (1982) Clay Min 17:175–183
3. Brindley GW, Moll WF (1965) Am Miner 50:1355–1370
4. Lambert JF, Deng Z, d'Espinase JB, Fripiat JJ (1989) J Coll Interface Sci 132:337–351
5. Williams S, Becerro AI, Castro MA, Thomas RK (1997) Physica B 234–236:1096–1098
6. Lagaly G (1986) Solid State Ionics 22:43–51
7. Grandin A, Borel MM, Raveau B (1985) J Solid State Chem 60:366–375
8. Lagaly G (1976) Angew Chem Int Ed Engl 15:575–586
9. Farmer VC, Russell JD (1964) Spectrochim Acta 20:1149–1173
10. Olejnik S, Aylmore LAG, Posner AM, Quirk JP (1968) J Phys Chem 72: 241–249
11. Kristof J, Mink J, Horvath E, Gabor M (1993) Vibrational Spectroscopy 5:61–67
12. Snyder RG (1961) J Mol Spectrosc 7:116–144
13. Snyder RG, Hsu SL, Krimm S (1978) Spectrochim Acta 34A:395–406
14. Snyder RG, Strauss HL, Elliger CA (1982) J Phys Chem 86:5145–5150
15. MacPhail RA, Strauss HL, Snyder RG, Elliger CA (1984) J Phys Chem 88: 334–341
16. Maroncelli M, Qi SP, Strauss HL, Snyder RG (1982) J Am Chem Soc 104:6237–6247
17. Casal HL, Mantsch HH (1984) Biochim et Biophys Acta 779:381–401
18. Hübner W, Mantsch HH (1991) Biophys J 59:1261–1272
19. Kodati VR, El-Jastimi R, Lafleur M (1994) J Phys Chem 98: 12191–12197
20. Fringeli UP, Günthard HH (1981) Molecular Biology, Biochemistry and Biophysics 31:270–332
21. Chao KJ, Wu CN, Chang H, Lee LJ, Hu S-f (1997) J Phys Chem B 101: 6341–6349
22. Bergk K-H, Schwieger W, Porsch M (1987) Chem Technol 39:459–466
23. Bergk K-H, Schwieger W, Porsch M (1987) Chem Technol 39:508–514
24. Binder H, Anikin A, Kohlstrunk B, Klose G (1997) J Phys Chem B 101:6618–6628
25. Harrick NJ (1967) Internal Reflection Spectoscopy. Wiley, New York
26. Schröder H, Neuroth N (1967) Optik 26:381–402
27. Flach CR, Gericke A, Mendelsohn R (1997) J Phys Chem B 101:58–65
28. Schwieger W, Heidemann D, Bergk K-H (1985) Rev Chim Minerals 22:639–650
29. Lazarev AH, Tenischewa TF (1962) Optika i Spektroskopija 12:215–219
30. Snyder RG, Goh MC, Srivatsovoy VJP, Strauss HL, Dorset DL (1992) J Phys Chem 96:10 008–10 019
31. Wong PTT, Siminovitch DJ, Mantsch HH (1988) Biochim et Biophys Acta 947:139–171
32. Snyder RG, Liang GL, Strauss HL, Mendelsohn R (1996) Biophys J 71: 3186–3198
33. Saupe A, Maier W (1961) Z Naturf 16a:816–824
34. Kiefer R, Baur G (1989) Mol Cryst Liq Cryst 174:101–126
35. Holland RF, Nielsen JR (1962) J Mol Spectrosc 8:383–405
36. Rand P (1981) Ann Rev Biophys Bioeng 10:277–314
37. Chen Y-L, Israelachvili JN (1992) J Phys Chem 96:7752–7760
38. Binder H, Gutberlet T, Anikin A, Klose G (1998) Biophys J 74:1908–1923
39. Small DM (1986) The Physical Chemistry of Lipids. Plenum Press, New York and London
40. Rand RP, Parsegian VA (1989) Biochim et Biophys Acta 988:351–376
41. Pascher I, Lundmark M, Nyholm P-G, Sundell S (1992) Biochim Biophys Acta 1113:339–373
42. McIntosh TJ (1980) Biophys J 29: 237–246
43. Lunden B-M (1974) Acta Crystallogr B 30:1756
44. Schwieger W, unpublished results